An Irradiance-Independent, Robust Ground-Fault Detection Scheme for PV Arrays Based on Spread Spectrum Time-Domain Reflectometry (SSTDR)

Sourov Roy, *Student Member, IEEE*, Mohammed Khorshed Alam, *Member, IEEE*, Faisal Khan, *Senior Member, IEEE*, Jay Johnson, *Member, IEEE*, and Jack Flicker, *Member, IEEE*

***Abstract*—A healthy photovoltaic (PV) array has a specific impedance between node pairs, and any ground fault changes the impedance values. Reflectometry is a well-known technique in electromagnetics, and it could be exploited to detect fault and aging-related impedance variations in a PV system. A fault detection algorithm using the spread spectrum time-domain reflectometry (SSTDR) method has been introduced in this paper. SSTDR has been successfully used for detecting and locating aircraft wiring faults. However, the wide variation in impedance throughout the entire PV system, which is caused by the use of different materials and interconnections makes PV fault detection more challenging while using reflectometry. Unlike other conventional ground-fault detection techniques specifically developed for PV arrays, SSTDR does not depend on fault-current magnitudes. Therefore, SSTDR can be used even in the absence of the solar irradiation, which makes it a very powerful fault-detection tool. The proposed PV ground-fault detection technique has been tested in a real-world PV system, and it can confidently detect PV ground faults for different configurations of PV arrays (single and double strings) and fault resistances (0.5, 5, and 10-Ω). Moreover, it has been experimentally verified that our proposed algorithm works at low irradiance and can detect specific ground faults that may remain undetected using the conventional ground-fault detection and interrupter (GFDI) fuses.**

***Index Terms*—Correlation, fault impedance, fault detection, ground-fault detection and interrupter (GFDI), grounding, interconnect, Photovoltaic (PV), PV array, reflectometry, spread spectrum time-domain reflectometry (SSTDR).**

I. Introduction

PHOTOVOLTAIC (PV) installation throughout the world has been exponentially increasing, and the total installed capacity of PV power globally reached more than 303 GW in 2016 from 1.3 GW in 2000, which covers at least 1.8% of the world electricity demand [1]. This rapid development of the PV system has made its fault detection and isolation absolutely necessary to avoid catastrophic failure in the power system. Based on their locations, three types of failures in PV systems are studied in power electronics: faults on PV arrays [2]–[24], failures in power conditioning systems [25]–[30], and disturbances in the utility interconnections (such as islanding, and so on) [31]–[34]. However, recent fire events initiated by the catastrophic failures in PV arrays have been drawing attention of researchers toward this area [9], [10]. Among all possible major faults that happen in the PV arrays such as ground faults, line-to-line faults [2]–[21], arc faults [22], [23], hot-spot formation [24], open circuit faults [18], [19], ground faults are considered to be the most common faults in PV systems. The ground fault is the undesirable condition of current flowing through the unintentional low-resistance path between a current-carrying conductor (CCC) and an equipment grounding conductor (EGC)/earth. In addition to CCCs, a PV array has several noncurrent-carrying conductors (NCCCs) such as module frames, mounting racks, metal enclosures, distribution panels, the chassis of end-use appliances, and power converters. No current flows through these paths under normal operating conditions, but a nonzero current exists in any path during faults. All these NCCCs are connected through the EGC, and the use of EGC is mandated by National Electrical Code 690.43 regardless of the nominal voltage of the PV system [35]–[38].

PV array installations can be divided into two categories: grounded and ungrounded [36]–[39]. In grounded systems, at least, one of the CCCs needs to be connected to the EGC using a ground-fault detection and interrupter (GFDI) fuse in order to detect the presence of any accidental circulating current path, and this is termed as system grounding. PV systems with system grounding are known as grounded, and this category is prevalent in the U.S.; an example of this grounding type is illustrated in Fig. 1. However, there are alternative ground-fault protection schemes, which are more common outside the U.S. including residual current monitoring devices (RCD) and dc insulation resistance (Riso) measurements [4], [5]. These ground-fault protection systems often are used on ungrounded (floating) PV systems that do not have a connection between a CCC and ground.

These ground-fault protection devices suffer from several limitations. For instance, a ground fault may remain undetected

Manuscript received June 7, 2017; revised August 10, 2017; accepted September 5, 2017. Date of publication September 20, 2017; date of current version April 20, 2018. Recommended for publication by Associate Editor Dr. Y. Li. *(Corresponding author: Sourov Roy.)*

S. Roy and F. Khan are with the Department of Computer Science and Electrical Engineering, University of Missouri-Kansas City, Kansas City, MO 64110 USA (e-mail: srdh9@mail.umkc.edu; faisal.khan@umkc.edu).

M. K. Alam is with Ford Motor Company, Dearborn, MI 48126 USA (e-mail: khorshed.alam@utah.edu).

J. Johnson and J. Flicker are with the Sandia National Laboratories, Albuquerque, NM 87123 USA (e-mail: jjohns2@sandia.gov; jdflick@sandia.gov).

Color versions of one or more of the figures in this paper are available online at http://ieeexplore.ieee.org.

Digital Object Identifier 10.1109/TPEL.2017.2755592

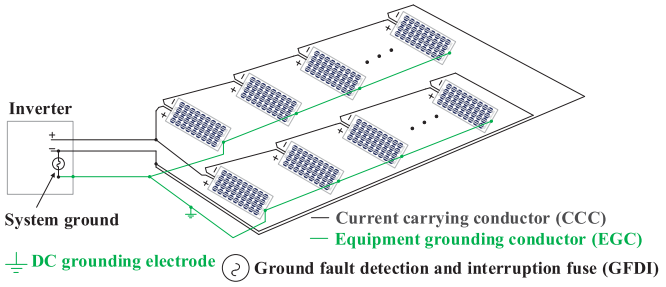

Fig. 1. Typical grounding diagram of PV arrays. The GFDI fuse (system ground) is usually installed inside the PV inverter in a grounded PV array, and system grounding is absent in an ungrounded PV array.

when the fault current falls within the blind spot range because of the low irradiance and high fault impedances [4], [5], [7], [8]. This phenomenon is known as the blind spot of the detection device, i.e., when the fault current magnitude is less than the tripping/melting current of this device preset [7], [8]. Recent fire events on April 5, 2009 in Bakersfield, CA, USA and April 16, 2011 in Mount Holly, NC, USA, resulted from undetected ground faults within the blind spot range. In both of these fire events, a double ground fault occurred. The first ground fault occurred between the negative CCC and EGC and resulted in current flow through the GFDI fuse, although the current magnitude was below the rated current of the installed fuse, and this fault remained undetected for indefinite amount of time. The second ground fault within the same array resulted in a flow of 952 A of current through the EGC and ignited fire before the fault current was cleared by the overcurrent protection fuse [9], [10].

Apart from ground-fault detection devices, several ground-fault detection techniques have been proposed in recent years that are based on comparisons of estimated and measured variables, pattern recognition using signal processing, machine learning analysis, and so on. Platon *et al.* [11] proposed an online fault detection method based on the differences between measured and estimated ac power output from a modeled PV system. A "fractional-order color relation classification" based fault detection method has been introduced in [12] where a fractional-order dynamic error (FODE) is calculated to measure the power degradation caused by the fault. In [13], a "descriptive and inferential statistic" has been conducted on the population of the energy generated from the PV inverters equipped with each PV subarray to identify the faulty part of the plant. A wireless-sensor-based fault detection technique, which detects fault by comparing expected values with measured values of operating voltages and currents of PV panels, is introduced in [14] and [15]. A fault diagnosis technique for the PV panel is presented in [16], where several intrinsic parameters are estimated based on modified particle swarm optimization (MPSO) by sampling the dynamic panel voltage and current. The fault in the panel can be detected if there is any change in the estimated parameters from their initial values. Saleh *et al.* [17] presented a fault detection method, based on the magnitudes and wave-shape characteristics of voltage signals of the PV modules, which needs two voltage transducers in each string. All of these methods are computation intensive and need external sensors to collect the data. Moreover, machine-learning techniques based on prerecorded and on-site data have been proposed in [18] and [19] and require a large amount of training data along with external sensors. Again, both the machine-learning-based and comparison-based fault detection techniques need accurate PV models to estimate circuit parameters. However, the models designed for specific environmental conditions are not capable of simulating the characteristics of the PV performance under different environmental conditions, and thus, may result in false detection in these cases [6], [18], [19], [40]–[42]. Therefore, these models have to be configured properly to get correct estimated values. Yi and Etemadi [20] presented a pattern-recognition-based fault detection method that utilizes fuzzy inference systems (FIS) to detect fault with the help of extracted necessary signal features from a multiresolution signal decomposition (MSD) technique. Though this method uses less sensors compared to the machine learning methods, it needs a series of filters that make the system more expensive. Authors of [21] utilized the difference in voltages between the healthy module in the faulty string and the module in the healthy string to locate the faulty module. This computation intensive method needs to update the software programs of the existing commercial converters with added additional voltage sensors. The authors of [6] proposed a high-impedance ground-fault (HIGF) detection scheme of PV arrays using the common-mode (CM) current spectrums of the CM model of the full-bridge inverter. This model-based fault detection technique needs to be updated for different configurations of PV arrays and experiences difficulties in determining the stray and parasitic parameters.

Most of these existing ground fault detection techniques require several on-site parameters such as voltage, current, generated power, irradiance level, temperature, humidity, etc., for accurate fault detection, and changes in any of these parameters may affect the *I–V* characteristics/MPPT of the PV panel [2], [4], [43]–[47]. Moreover, nonuniform irradiance levels (i.e., partial shading, etc.) and bypass diodes have a significant impact on the *I–V* characteristics/MPPT scheme of the PV panel [2], [48]–[51], and thus, make the fault detection techniques more challenging especially for those methods that rely on the *I–V* characteristics of the PV module.

To overcome these limitations in PV array fault detection techniques, reflectometry methods might become a good candidate because these methods do not use traditional on-site parameters and sensors to detect faults [52]. However, different reflectometry methods have long been used for detection and locating faults in wires, and a comparative study summarizing different reflectometry methods for fault detection in electrical wiring was discussed in [52]. Among known reflectometry techniques, spread spectrum time-domain reflectometry (SSTDR) provides several advantages over other reflectometry techniques such as low-cost fault detection in powered/live cables, very-high noise immunity, embedded solutions, etc. [52]–[56].

Potential benefits of using time-domain reflectometry for detecting faults in a PV array have already been explored in [57]–[61]. However, frequent changes in impedance throughout the PV array limit the success of fault detection schemes using reflectometry [60], [61]. It was concluded in [61] that the pres-

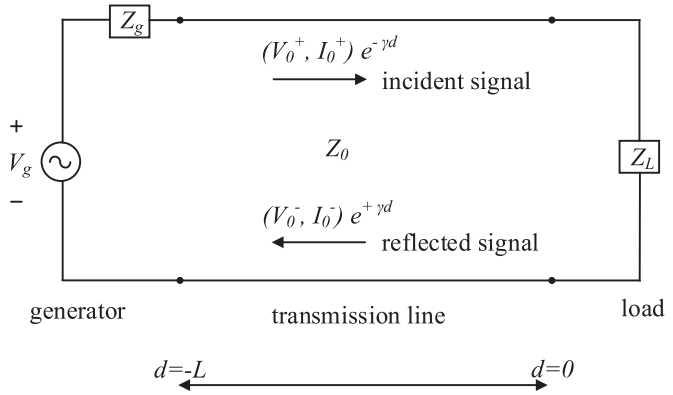

Fig. 2. Schematic diagram of a transmission line of length L and characteristic impedance equal to Z_0. A generator circuit is connected at one end ($d = -L$), and the other end ($d = 0$) is connected to load Z_L. An incident signal with voltage and current (V_0^+, I_0^+) is traveling toward the load, and a reflected signal with voltage and current (V_0^-, I_0^-) is traveling toward the generator.

ence of multiple reflections occurring at different mismatches makes interpretation of the time-domain reflection extremely difficult to detect the presence of a ground fault in PV arrays. The algorithm proposed in this paper demonstrates that SSTDR data can be implemented to overcome such limitations resulting in faithful detection of ground faults in PV arrays. Moreover, it is already mentioned that the conventional GFDI devices depend on fault current magnitude that may result within the blind spot range at night or low irradiance level. In contrast, rather than depending on the fault current magnitudes, SSDTR data are based on the impedance variation due to the ground fault. This unique feature makes SSTDR an excellent candidate for detecting ground fault when the fault current magnitude is less than the tripping current of the GFDI. In addition, comprehensive analysis have been conducted for the first time to investigate the impact of different parameters, i.e., carrier signal frequency, fault resistance, irradiance, number of faults, and number of strings on the observed result.

II. SSTDR

A. Basic Concepts of Reflectometry

Reflectometry is based on the reflection of an electrical signal at any impedance discontinuity in a transmission line. As illustrated in Fig. 2, any incident signal (V_0^+, I_0^+) travels through the transmission line, and a portion of the signal is reflected back (V_0^-, I_0^-) if it finds any impedance mismatch from the characteristic impedance (Z_0) of the line. Two important parameters of a transmission line are characteristic impedance (Z_0) and reflection coefficient (ρ). Characteristic impedance, Z_0, is defined as the ratio between the voltage and current of the incident or the reflected wave as follows [62]:

$$Z_0 = \sqrt{\frac{R' + j\omega L'}{G' + j\omega C'}} = \frac{V_0^+}{I_0^+} = \frac{V_0^-}{I_0^-} \tag{1}$$

where R'(Ω/m), L'(H/m), G'(S/m), and C'(F/m) are per unit length resistance, inductance, conductance, and capacitance of the transmission line, respectively. The ratio between the reflected and incident voltage signals is known as the reflection coefficient (ρ), which is a measurement of how much signal is reflected back [defined in (2)]

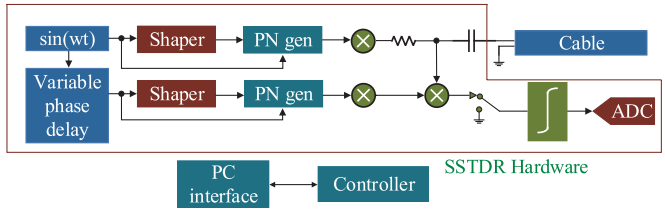

Fig. 3. Schematic diagram of the SSTDR hardware [53].

$$\rho = \frac{V_0^-}{V_0^+} = \frac{Z_L - Z_0}{Z_L + Z_0} \tag{2}$$

where Z_0 is the characteristic impedance and Z_L is the impedance at the point of fault. Generating an equivalent transmission-line model for a PV string/array is a mammoth task because of the presence of different materials and interconnections throughout the entire signal propagation path. Initiatives have been taken to develop the transmission-line model for PV modules considering only the metal connectors of a PV module in [61]. Transmission-line parameters will vary from one PV plant to another due to the use of different PV modules (solar cell material, shape, size, orientation of conducting ribbons, number of cells in a series, orientation of series-connected solar cells, design and material of the metal module, EGC connection variation, etc.), spatial orientation of modules, type and length of the EGC and CCCs, number of modules connected in a series, etc. Therefore, such an approach is not practical considering the amount of time and cost required to extract transmission-line parameters for each PV array.

B. SSTDR

SSTDR uses a pseudorandom binary signal called the pseudonoise code (PN code) as an incident signal, and it consists of randomly generated 1 and 0 s (each 1/0 is known as a chip) [52]–[56], [63]. SSTDR can be implemented in several ways as discussed in [53], [54], and [64]–[66], and a simple schematic diagram is shown in Fig. 3 .

The PN code is modulated with a carrier sine wave to generate the incident signal. The frequency of the carrier sine wave is also known as the center frequency of SSTDR. To calibrate the system without any difficulties, frequency of the carrier sine wave is maintained the same as well as the chip rate ($f_C = 1/T_C$) of the PN code [53], [54]. The reflected signal is cross correlated with the delayed copies of the incident signal with the help of a variable phase-delay generator. Any mismatch from the characteristic impedance at the load terminal generates a lobe at a time delay in the autocorrelation plot that corresponds to the distance from the source terminal. A lobe with a positive peak indicates a positive reflection coefficient ($\rho > 0$, if $Z_L > Z_0$) and a negative peak indicates a negative reflection coefficient ($\rho < 0$, if $Z_L < Z_0$).

An example of the SSTDR generated incident signal and corresponding fast Fourier transformation (FFT) is shown in Fig. 4.

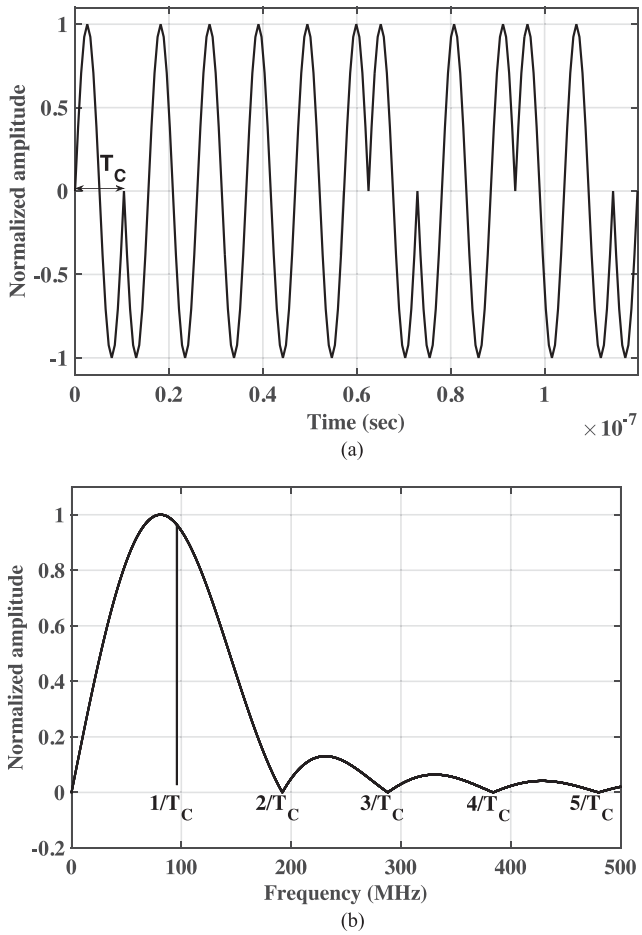

Fig. 4. Incident signal of SSTDR with carrier/center frequency equal to 96 MHz: (a) time-domain representation (a portion of one entire PN/SSTDR sequence is shown here). (b) frequency-domain (FFT) representation (only the upper side band is shown here).

The FFT of the PN code is similar to a sinc function where the width of the main lobe is twice the chip rate of the PN code. The Fourier transform of the incident signal is similar to double sideband suppressed carrier signal where the signal has a large spectral distribution since the sinusoidal signal has been used as the modulating signal here. From Fig. 4, it is evident that the main lobe shifts further away from 0 Hz once the center frequency increases. Since the power in the noise usually centered around 0 Hz, increasing the carrier frequency of SSTDR signal will lead to produce less power in the cross correlation of an SSTDR signal with noise, which will eventually increase the SNR of the system. A field-programmable-gate-array-based SSTDR generator (see Fig. 5) has been used in this paper. This hardware allows scanning the system connected to the hardware with center frequencies equal to 96, 48, 24, 12, 6, 3, 1.5, 0.75, and 0.375 MHz.

III. Ground-Fault Detection Using SSTDR

The proposed ground-fault detection algorithm was implemented at the Distributed Energy Technologies Laboratory (DETL) of Sandia National Laboratories (SNL) (see Fig. 6). A PV string consisting of seven, series-connected PV modules

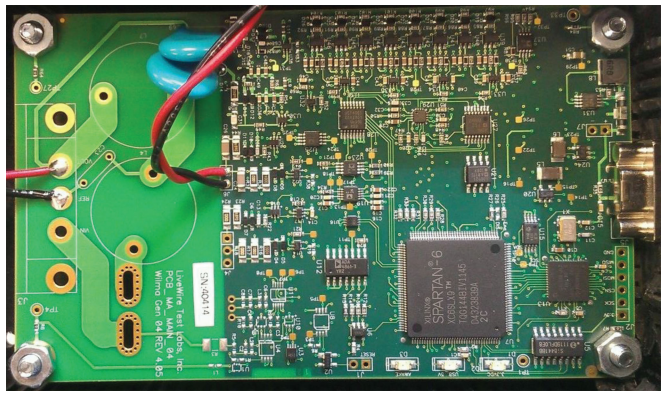

Fig. 5. WILMA LWG40414 SSTDR hardware device (An R&D product from Livewire Innovation).

Fig. 6. Facilities used at DETL of SNL to perform tests [5].

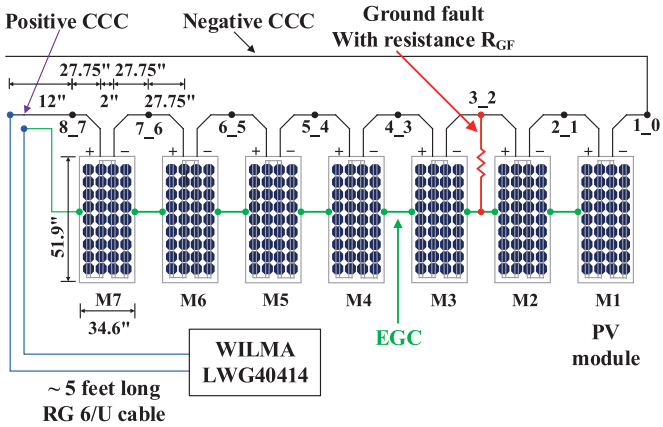

Fig. 7. Schematic diagram of the test setup (physical dimensions are not drawn according to scale).

from Sanyo was interfaced with the SSTDR hardware, as depicted in the schematic diagram in Fig. 7. The dimension of each module was 51.9 × 34.6 × 1.8 in. Each module was connected in series through 55.5-in cable, where each fault location was exactly halfway between the adjacent module. Specifications of the PV modules are listed in Table I. Output terminals of the SSTDR board were connected to the positive CCC and the EGC

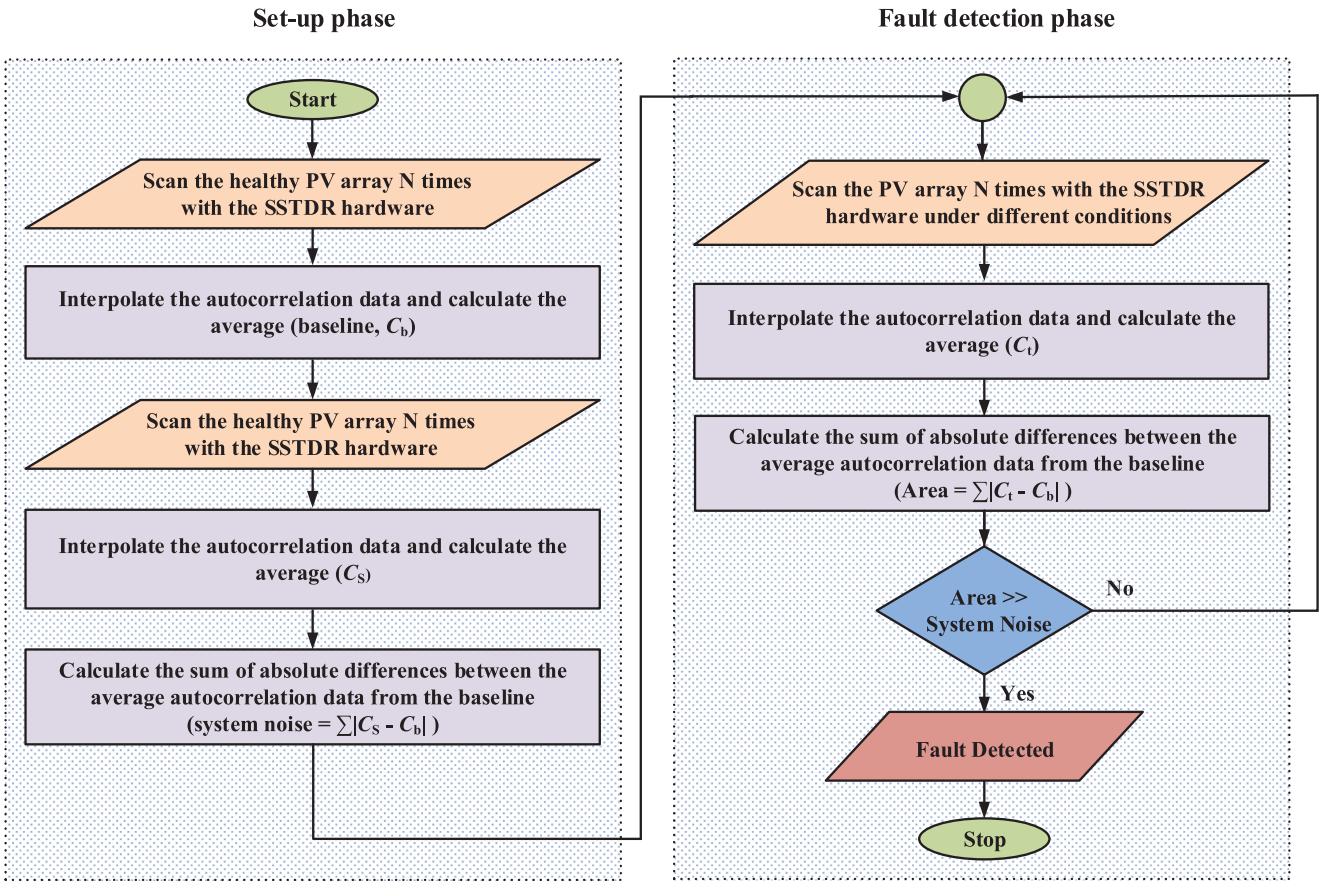

Fig. 8. Flowchart of the ground-fault detection algorithm.

TABLE I
SPECIFICATION OF A PV MODULE USED IN THE TEST SETUP (AT 1000 W/M^2, 25 °C CELL TEMPERATURE)

Maximum power (P_{max})	200 W
Short circuit current (I_{sc})	3.83 A
Open circuit voltage (V_{oc})	68.7 V
Maximum power current (I_{pmax})	3.59 A
Maximum power voltage (V_{pmax})	55.8 V

of the PV string. The ground-fault detection algorithm developed within the scope of this project is based on the three steps described in the following subsections, and a flowchart of this algorithm is shown in Fig. 8. In order to avoid needless disconnections during monitoring the system for ground faults, it is advisable to have the SSTDR system permanently connected to the device under test.

A. Creating Baseline

As mentioned earlier, every PV array has different reflection patterns, and it is necessary to create a baseline for each array under consideration. This will work as a reference to detect ground faults later. In order to create the autocorrelation baseline (C_b), the PV string without any ground fault was scanned in static mode for five times (i.e., $N = 5$), and autocorrelation plots were interpolated at the rate (M) of 10 using the interp() function in MATLAB. If C_i ($i = 1, 2, 3, 4, 5$) are the interpolated autocorrelation vectors, C_b is defined as

$$C_b = \frac{\sum_{i=1}^{N} C_i}{N}. \tag{3}$$

The baseline plot with a carrier/center frequency of 750 kHz is shown in Fig. 9. The abscissa of the autocorrelation plots have been represented in the form of time delay, since the velocity of propagation through the PV string is unknown and is expected to vary throughout the PV string. For our algorithm, the average of these five autocorrelation plots for each center frequency is considered as a baseline for differentiating PV array without ground fault (healthy PV array) and with ground fault. It should be noted that both the scan number (N) and interpolation rate (M) have been chosen arbitrarily, and time taken to create the autocorrelation baseline for each scan was approximately 4 ms. The net processing time for implementing the algorithm (except scanning the system) depends on the sampling rate and the computational speed of the digital signal processor block. However, a higher number of scans or interpolation rate is recommended provided the system can handle a big amount of data.

B. Estimating System Noise

The autocorrelation data generated by the SSTDR hardware for the same setup are not identical and show some variations, as

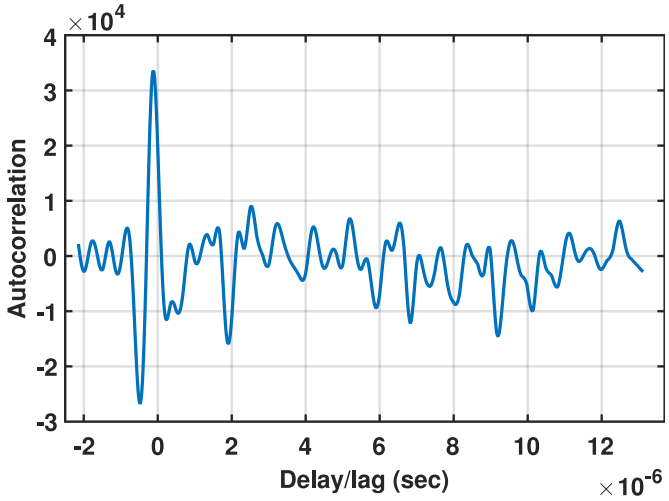

Fig. 9. Baseline autocorrelation plot for ground-fault detection with center frequency of 750 kHz.

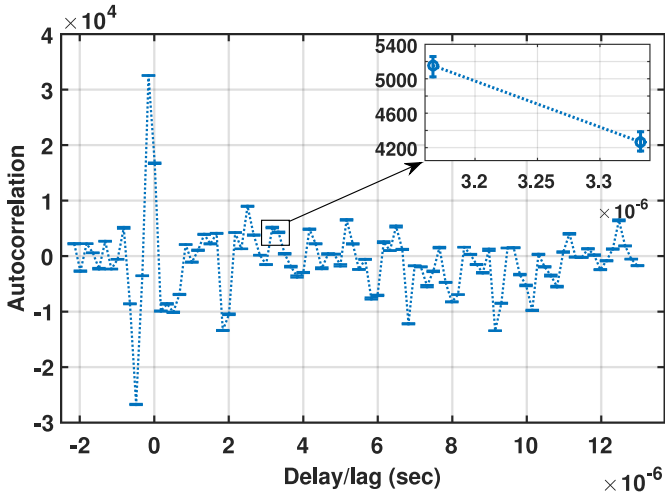

Fig. 10. Error plot of autocorrelation data for center frequency of 750 kHz.

shown in the error plot for a carrier frequency equal to 750 kHz in Fig. 10. These variations in the autocorrelation plot are expected because of the thermal noise, noise generated from the analog to digital conversion, etc. Considering this fact, SSTDR was applied N times to the same PV array, and the autocorrelation data were interpolated and averaged (C_s). Each baseline data point calculated in the previous subsection (C_b) was subtracted from the calculated average data, and the absolute values of the differences were considered. The sum of the absolute differences between the average autocorrelation data and the baseline is considered as an estimate of system noise (N_s) as shown in (4) since both values were collected for the same healthy PV string. To facilitate the real-time monitoring of the PV array, C_s needs to be periodically measured, and therefore, N_s will be updated accordingly

$$N_s = \sum_{i=1}^{k} | C_{s,i} - C_{b,i} |. \tag{4}$$

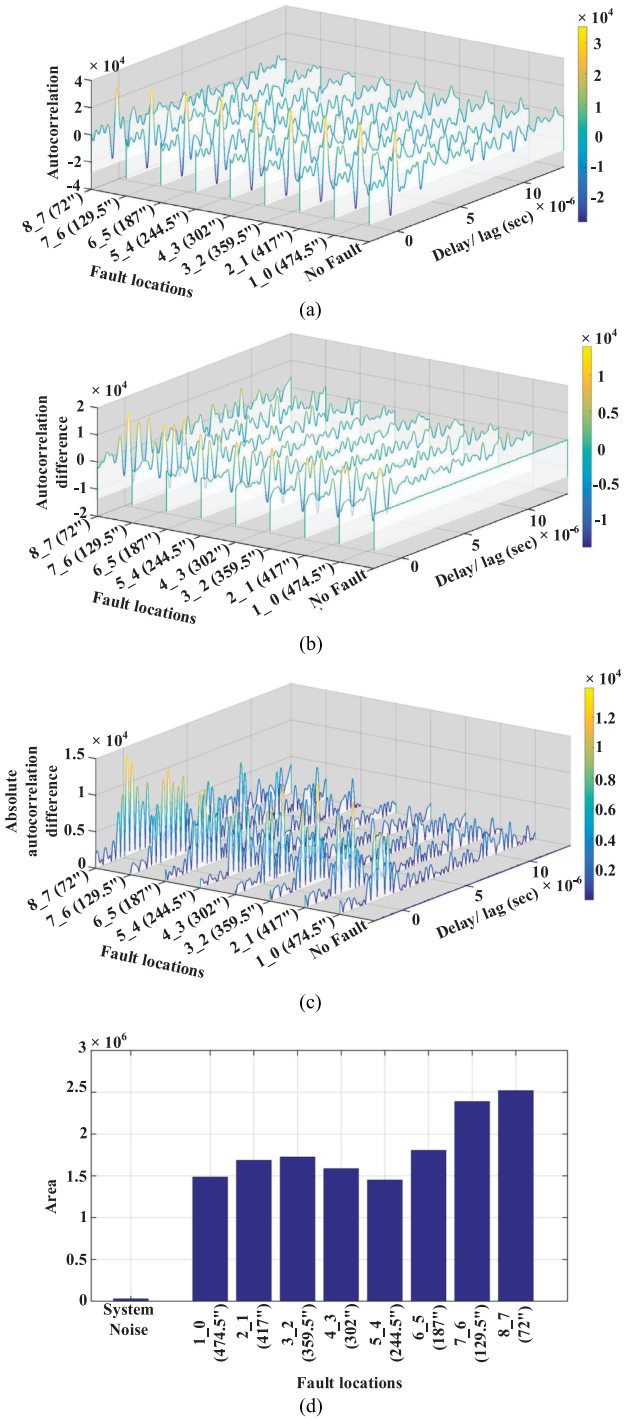

Fig. 11. (a) Average autocorrelation plot using the same PV string without any ground fault and ground fault at different locations, (b) difference between average autocorrelation data and the baseline, (c) absolute values of the differences, (d) sum of absolute values of the differences. Here, center frequency = 750 kHz and fault resistance = 0.5-Ω.

where subscript i represents ith element of corresponding autocorrelation vectors and k is the length of both vectors.

C. Fault Detection

Artificial ground faultswere created at different nodes between the modules using a 0.5-Ω fuse to validate the fault de-

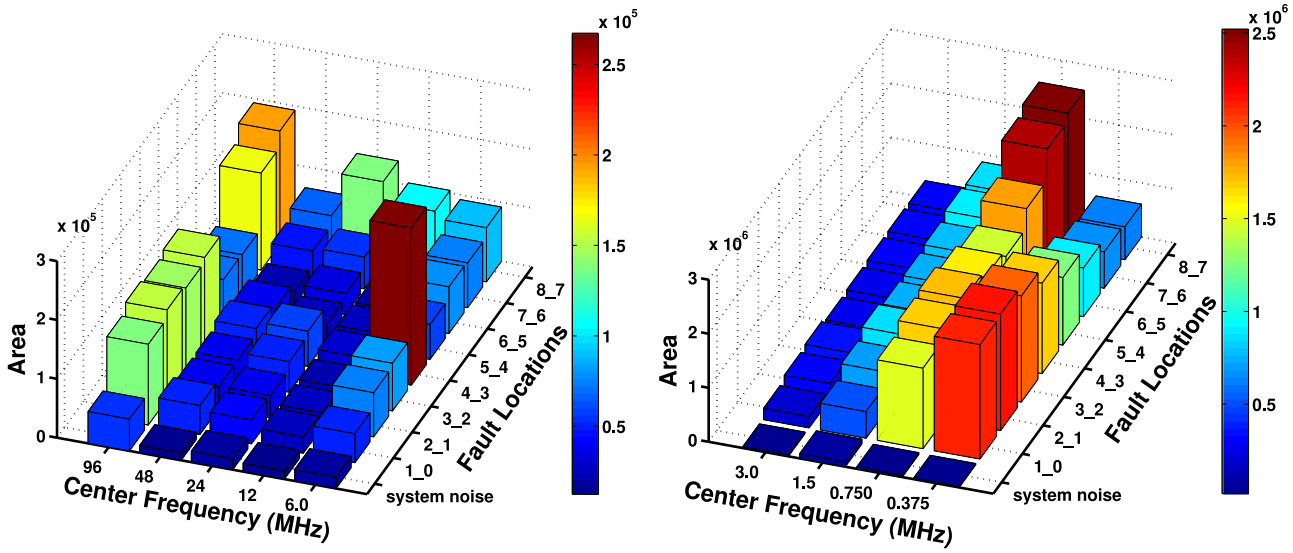

(a) (b)

Fig. 12. Area under absolute autocorrelation difference plots for healthy PV string (system noise) and ground faults at different locations in the PV string using 0.5-Ω resistor with different center frequencies: (a) center frequencies from 96 to 6 MHz and (b) center frequencies from 3 to 0.375 MHz.

tection algorithm. The PV string was scanned N times with ground faults at different nodes, as shown in Fig. 7, and the average autocorrelation plots (C_t) were generated for faults at different locations in the PV string. The absolute values of the element-wise differences between the average autocorrelation plot with ground fault in a specific location and the baseline were calculated, and the sum of these absolute differences has been termed as the "area" in this manuscript. The area (A), as defined in (5), for ground faults at different locations in the same PV string along with the system noise is shown in Fig. 11 for a center frequency equal to 750 kHz, and it was apparent that the PV array generates an area that is higher than the last updated system noise whenever there is a ground fault in the array

$$\text{area} = \sum_{i=1}^{k} \mid C_{t,i} - C_{b,i} \mid. \tag{5}$$

IV. Influence of Different Parameters on Fault Detection Algorithm

The autocorrelation data in an SSTDR-based fault detection method depends on numbers of parameters that affect the impedances (either Z_0 or Z_L) in the propagation paths of SSTDR signals. For instance, the number of connected strings (series or parallel), number of simultaneous faults, fault resistance, number of interconnections within the system, impedance variation throughout the array, PV cell material, metal conductors and frames of the PV module, and method by which SSTDR hardware is connected with the PV array, etc., lead to complex distributed capacitances and other parasitic components between the CCC and the ground. Since the algorithm is based on the differences between the average autocorrelation readings for the healthy and faulty PV array, the parameters that remain unchanged in both the healthy and faulty PV arrays, have little or no impact on the fault detection capability of the proposed algorithm. Moreover, the attenuation of the SSTDR signal depends on its velocity of propagation, distance to the fault, characteristic impedances of its propagation path, the length of the PN code, etc. [52]. Unfortunately, quantifying the impact of these parameters as well as the attenuation of SSDTR signal (where a large number of impedance variations and branch network is present throughout the PV array) is beyond the scope of this paper. The influence of different parameters, i.e., the center frequency of SSTDR, fault resistance, solar irradiance (to test the feasibility of fault detection at night and during cloudy days), parallel strings, and double ground fault on the robustness of the algorithm are discussed in this section.

A. Impact of Carrier Frequency

The spectral distribution of the signal is highly dependent on the carrier frequency because the generated PN code and the chip rate of the PN code vary in proportion to the carrier frequency [53], [54]. The width of the main lobe of the Fourier transform of the incident signal is twice the carrier frequency, and most of the energy of the incident signal is confined within that bandwidth. The power density of the incident signal spreads over a wider bandwidth with an increase in carrier frequency, and thereby, the response (reflected signal) is expected to vary with the variation in the carrier frequency.

The area under the absolute average autocorrelation difference plots for the same PV string with ground faults at different nodes (for different SSTDR carrier frequencies) and fault resistance equal to 0.5-Ω are shown in Fig. 12. Since the lower frequency signals travel further into the system, and the SSTDR signals need to propagate through both long cables and (lossy) PV modules, carrier frequencies lower than 6 MHz produce more reliable results compared to higher carrier frequencies for ground faults in the PV string. As an example, in Fig. 12(a), the area with ground faults is lowest at location 6_5 and it is only

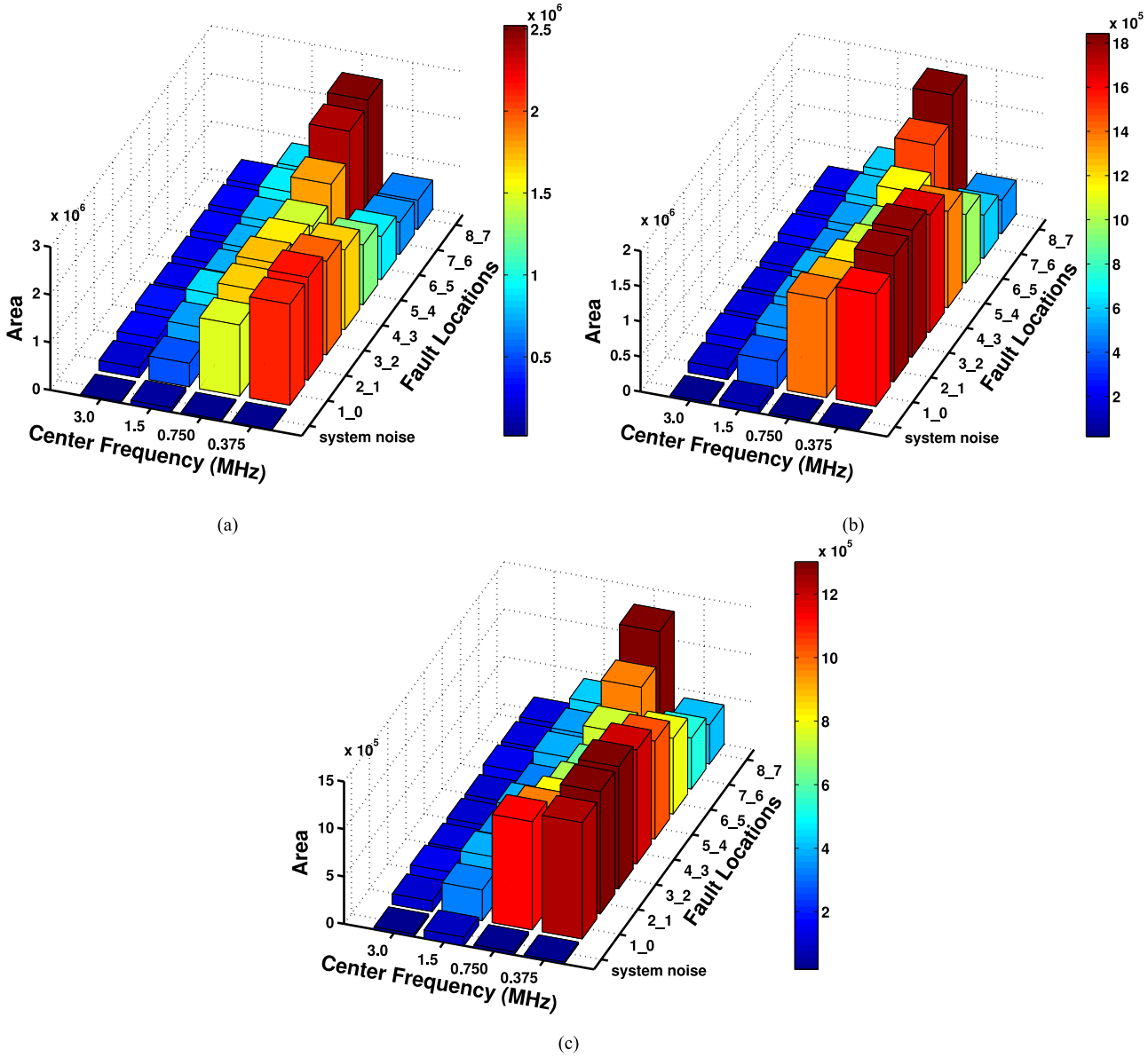

Fig. 13. Area plots for center frequencies 3.0, 1.5, 0.75, 0.375 MHz and fault resistances: (a) 0.5-Ω, (b) 5-Ω, (c) 10-Ω.

1.29 (approx.) times the system noise for a center frequency equal to 96 MHz. For 6, 3, 1.5, 0.7, and 0.375 MHz, these ratios are about 2.5, 7.96, 5.54, 48.04, and 31.89, respectively.

An extensive impedance domain mapping is required to explain the pattern of variation in areas at different locations. However, we decided to concentrate on the center frequency range of 375 kHz–3 MHz so that no erroneous fault is detected by the system.

B. Impact of Fault Resistance

The ground-fault resistance is an important aspect in a fault detection scheme since it may create a fault within the blind spot of the GFDI fuse. Ground faults usually range from tenth of an ohm to tens of kiloohms depending on the reason behind the onset of the fault [8]. High-resistance faults may happens due to corrosion bridge or insulation failure, and their impedance degrades over time. Moreover, high-impedance fault current may not be high enough to cause significant damage to the system and may easily go undetected. In fact, the fault current of lower magnitude under low irradiance level, which might go undetected, can be high enough to cause catastrophic damage due to added current of subsequent faults. In contrast, low-resistance fault increases the current through the fault path, which eventually increases the possibility of a fire. Moreover, the high-resistance fault current remains almost the same at different irradiance levels; whereas current in low-impedance fault path linearly changes with higher irradiance making the fault detection even more critical [8]. Therefore, within the scope of this research, low-resistance ground faults were created at different locations in the PV string for the following fault resistances: 0.5, 5, and 10-Ω. The autocorrelation area plots for different fault resistances and center frequencies (375 kHz–3 MHz) are shown in Fig. 13. The same baseline and system noise were used for all fault resistances since these two parameters (baseline and system noise) are independent of the fault resistance. A healthy PV

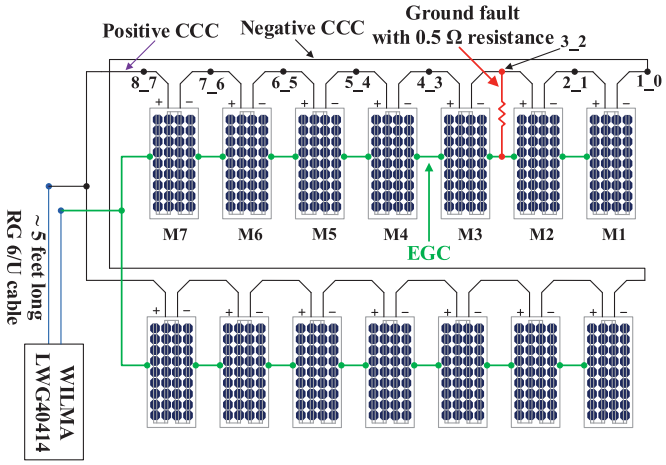

Fig. 14. Schematic diagram of the test setup for two parallel strings.

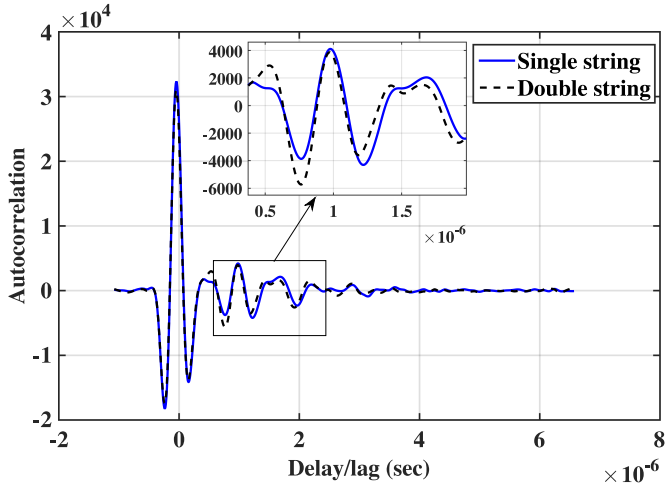

Fig. 15. Comparison of baseline autocorrelation plots for single string and double strings.

string has a very high resistance from any point on the CCCs to the EGC (greater than the fault resistances), which will lead to the value of reflection coefficient, ρ less than 0 (zero) [from (2)]. Therefore, it is expected that the area under the autocorrelation plot will decrease with the increase in fault resistance for the same center frequency and fault location.

The experimental results revealed that the overall area under the curve typically decreases once the fault impedance goes up. As an example, with a center frequency equal to 0.75 MHz and fault location 5_4, the area decreases from 1.451×10^6 for 0.5-Ω to 0.9529×10^6 for 5-Ω, and then, to 0.6221×10^6 for 10-Ω fault resistance. Even at 10-Ω fault impedance, the area under the curve was 20.59 times higher than the system noise of 0.9529×10^6. This indicates that the proposed algorithm can detect faults even with a very high fault impedance. The travel paths of SSTDR incident and reflected signals are different for faults at different locations, and the propagation velocity throughout the PV string can be different too. Therefore, the position of the autocorrelated amplitudes, and thus, the autocorrelated area will be different for different locations. That being said, the experimental results summarized in this paper conclude that the presence of a ground fault can be confidently detected for center frequencies less than 6 MHz regardless of the fault resistance (0.5 , 5, and 10-Ω).

C. Impact of Parallel-Connected Strings

In a larger PV array, it is expected that there will be several PV strings connected in parallel, and it may not be feasible to disconnect all the parallel strings for ground-fault detection purposes. In order to verify the algorithm, two PV strings were connected in parallel at the same facility, shown in Fig. 6, and ground faults were created at different interconnecting nodes in one of the PV strings using a 0.5-Ω resistor, as depicted in Fig. 14. Baseline autocorrelation plots for single string and two parallel strings without any ground fault are shown in Fig. 15 for center frequency 1.5 MHz, and there are some differences observed between these plots. Ground faults were created in one of the parallel strings, and area plots for different center frequencies (0.375–3 MHz) are shown in Fig. 16.

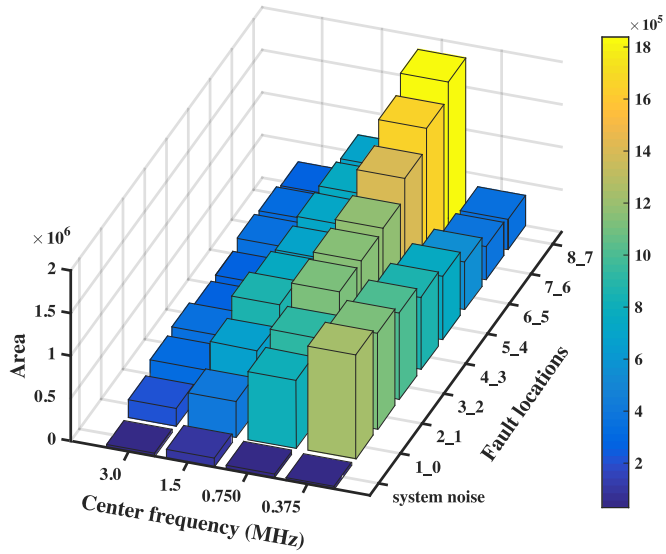

Fig. 16. Area plot for PV array consists of two parallel strings with and without ground faults.

In every fault condition, the area plot height is significantly higher than the system noise (no fault). Therefore, it can be concluded from the 3-D bar plot that SSTDR can be used for ground-fault detection in parallel-connected PV modules as effectively as in single PV strings. It is possible to locate the string with the PV fault using SSTDR, since the algorithm can detect the ground fault in parallel-connected strings, and each string can be examined with respect to its own baseline by disconnecting the parallel connection to detect ground faults after a ground fault has been observed in the array.

D. Impact of Solar Irradiance

Nominal changes occur in the electrical equivalent impedance of the solar cells when there is a change in solar irradiance, and this works in favor of the reflectometry-based fault detection schemes. In order to investigate the feasibility of ground fault detection using SSTDR at night or with low irradiance, a test was performed in a laboratory environment (<5-W/m^2 solar

TABLE II
SPECIFICATION OF A 100 W PV MODULE USED INSIDE THE LAB SETUP (AT 1000 W/M^2, 25 °C CELL TEMPERATURE)

Maximum power (P_{max})	100 W
Short circuit current (I_{sc})	5.75 A
Open circuit voltage (V_{oc})	22.5 V
Maximum power current (I_{pmax})	5.29 A
Maximum power voltage (V_{pmax})	18.9 V

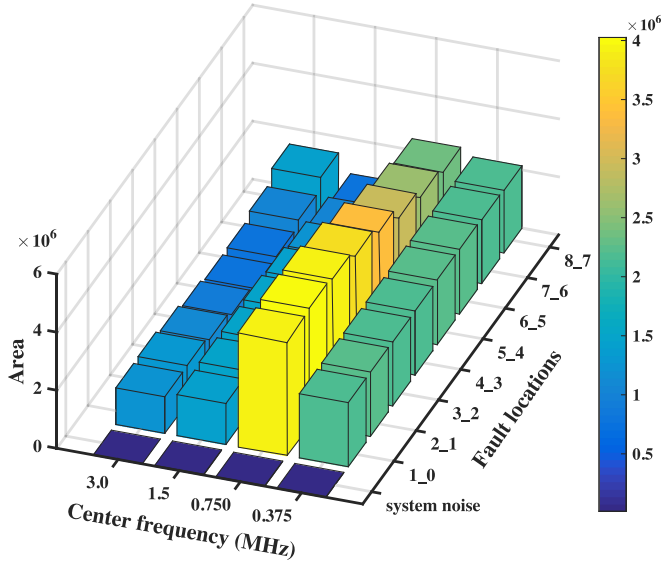

Fig. 17. Area plot for PV string inside laboratory with and without ground faults.

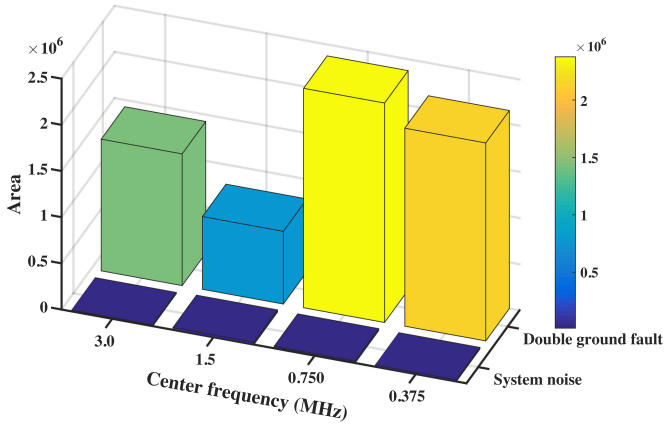

Fig. 18. Area plot for PV string with and without double ground fault for different center frequencies.

irradiance) with a PV string consisting of seven 100-W series-connected PV modules. Specifications of the PV modules are provided in Table II. A test setup similar to the schematic shown in Fig. 7 was built, and ground faults were created at different nodes by creating a short-circuit connection. Similar tests were performed as described in Section III, and the results are shown in Fig. 17.

It should be noted that the PV modules used inside the laboratory were smaller than the outdoor PV modules. Therefore, we expected them to have different patterns for the same carrier frequency since the equivalent lumped-circuit parameters ($R^{'}$, $L^{'}$, $G^{'}$, and $C^{'}$) were different. However, it can be concluded from Fig. 17 that the proposed algorithm can be used for ground-fault detection at very low irradiance as confidently as in an outdoor environment.

E. Double Ground Fault

A double ground-fault test was performed using the same PV string described in Section IV-D inside the laboratory facility, since it is not safe to create a double ground fault in an outdoor PV string. However, a double ground fault may occur in a real PV system when a ground fault remains undetected and another fault occurs at night. During the indoor experiment, two short circuits were created at 8_7 and 6_5 (arbitrarily chosen locations) positions and the PV string was scanned using the SSTDR hardware. A double ground generates a higher area under the absolute autocorrelation difference plot than the system noise and can be detected confidently, as shown in Fig. 18.

V. CONCLUSION

A novel SSTDR-based ground-fault detection algorithm has been presented in this paper. Detection of ground faults in PV arrays using reflectometry is challenging because hundreds of interconnections and impedance mismatches exist inside a single PV string. The proposed algorithm has been successfully used for detecting ground faults in PV arrays. Moreover, this technique can be implemented for testing ground faults at night or at low illumination, i.e., when the PV array is expected to generate no power. This unique feature makes the proposed technique extremely powerful and effective compared to any existing methods. This paper has presented the feasibility of using the SSTDR-based algorithm with any variation in the number of strings, fault resistance and number of faults, and the proposed method can effectively detect complex fault conditions as well. Based on the finding through various research projects pertinent to SSTDR, it is expected that this SSTDR-based fault detection scheme will create a new standard in the power engineering community.

ACKNOWLEDGMENT

The authors would like to thank Sandia National Laboratory for their support toward this project.

REFERENCES

[1] International Energy Agency, "Snapshot of global photovoltaic markets 2016," International Energy Agency Photovoltaic Power Systems Programme, Rep. IEA-PVPS T1-31:2017, 2016.
[2] Y. Zhao, J. F. de Palma, J. Mosesian, R. Lyons, and B. Lehman, "Line-line fault analysis and protection challenges in solar photovoltaic arrays," *IEEE Trans. Ind. Electron.*, vol. 60, no. 9, pp. 3784–3795, Sep. 2013, doi: 10.1109/TIE.2012.2205355.
[3] Y. Zhao, B. Lehman, J. F. DePalma, J. Mosesian, and R. Lyons, "Fault evolution in photovoltaic array during night-to-day transition," in *Proc. 2010 IEEE 12th Workshop Control Model. Power Electron.*, Jun. 2010, pp. 1–6, doi: 10.1109/COMPEL.2010.5562434.
[4] M. K. Alam, F. Khan, J. Johnson, and J. Flicker, "A comprehensive review of catastrophic faults in PV arrays: Types, detection, and mitigation techniques," *IEEE J. Photovolt.*, vol. 5, vol. 3, pp. 982–997, May 2015, doi: 10.1109/JPHOTOV.2015.2397599.

[5] M. K. Alam, F. Khan, J. Johnson, and J. Flicker, "PV ground-fault detection using spread spectrum time domain reflectometry (SSTDR)," in *Proc. 2013 IEEE Energy Convers. Congr. Expo.*, Sep. 2013, pp. 1015–102, doi: 10.1109/ECCE.2013.6646814.

[6] G. Wang, C. C. Youn, and A. M. Stankovic, "DC-side high impedance ground fault detection for transformerless single-phase PV systems," in *Proc. North Amer. Power Symp.*, Oct. 2015, pp. 1–6, doi: 10.1109/NAPS.2015.7335209.

[7] J. Flicker and J. Johnson, "Analysis of fuses for blind spot ground fault detection in photovoltaic power systems," Sandia National Laboratories, Albuquerque, NM, USA, Tech. Rep., 2013. [Online]. Available: http://www.solarabcs.org/about/publications/reports/blindspot/pdfs/analysis_of_fuses-June-2013.pdf

[8] J. Flicker and J. Johnson, "Photovoltaic ground fault and blind spot electrical simulations," Sandia National Laboratories, Albuquerque, NM, USA, Tech. Rep. SAND2013-3459, 2013.

[9] B. Brooks, "The bakersfield fire: A lesson in ground-fault protection," *Solar Pro Mag.*, vol. 4, vol. 2, pp. 62–70, Feb./Mar. 2011.

[10] B. Brooks, "The ground-fault protection blind spot: Safety concern for larger PV systems in the US," Solar American Board for Codes and Standards, 2012. [Online]. Available: http://www.solarabcs.org/about/publications/reports/blindspot/pdfs/BlindSpot.pdf

[11] R. Platon, J. Martel, N. Woodruff, and T. Y. Chau, "Online fault detection in PV systems," *IEEE Trans. Sustain. Energy*, vol. 6, vol. 4, pp. 1200–1207, Oct. 2015, doi: 10.1109/TSTE.2015.2421447.

[12] C. L. Kuo, J. L. Chen, S. J. Chen, C. C. Kao, H. T. Yau, and C. H. Lin, "Photovoltaic energy conversion system fault detection using fractional-order color relation classifier in microdistribution systems," *IEEE Trans. Smart Grid*, vol. 8, vol. 3, pp. 1163–1172, May 2017, doi: 10.1109/TSG.2015.2478855.

[13] S. Vergura, G. Acciani, V. Amoruso, G. E. Patrono, and F. Vacca, "Descriptive and inferential statistics for supervising and monitoring the operation of PV plants," *IEEE Trans. Ind. Electron.*, vol. 56, vol. 11, pp. 4456–4464, Nov. 2009, doi: 10.1109/TIE.2008.927404.

[14] B. Andò, S. Baglio, A. Pistorio, G. M. Tina, and C. Ventura, "Sentinella: Smart monitoring of photovoltaic systems at panel level," *IEEE Trans. Instrum. Meas.*, vol. 64, no. 8, pp. 2188–2199, Aug. 2015.

[15] P. Guerriero, F. D. Napoli, G. Vallone, V. d'Alessandro, and S. Daliento, "Monitoring and diagnostics of PV plants by a wireless self-powered sensor for individual panels," *IEEE J. Photovolt.*, vol. 6, vol. 1, pp. 286–294, Jan. 2016, doi: 10.1109/JPHOTOV.2015.2484961.

[16] W. Wang, A. C. F. Liu, H. S. H. Chung, R. W. H. Lau, J. Zhang, and A. W. L. Lo, "Fault diagnosis of photovoltaic panels using dynamic current-voltage characteristics," *IEEE Trans. Power Electron.*, vol. 31, vol. 2, pp. 1588–1599, Feb. 2016, doi: 10.1109/TPEL.2015.2424079.

[17] K. A. Saleh, A. Hooshyar, E. F. El-Saadany, and H. H. Zeineldin, "Voltage-based protection scheme for faults within utility-scale photovoltaic arrays," in *IEEE Trans. Smart Grid*, vol. PP, no. 99, pp. 1–1. doi: 10.1109/TSG.2017.2655444.

[18] M. N. Akram and S. Lotfifard, "Modeling and health monitoring of dc side of photovoltaic array," *IEEE Trans. Sustain. Energy*, vol. 6, vol. 4, pp. 1245–1253, Oct. 2015, doi: 10.1109/TSTE.2015.2425791.

[19] Y. Zhao, R. Ball, J. Mosesian, J. F. de Palma, and B. Lehman, "Graph-based semi-supervised learning for fault detection and classification in solar photovoltaic arrays," *IEEE Trans. Power Electron.*, vol. 30, vol. 5, pp. 2848–2858, May 2015, doi: 10.1109/TPEL.2014.2364203.

[20] Z. Yi and A. H. Etemadi, "Fault detection for photovoltaic systems based on multi-resolution signal decomposition and fuzzy inference systems," *IEEE Trans. Smart Grid*, vol. 8, vol. 3, pp. 1274–1283, May 2017, doi: 10.1109/TSG.2016.2587244.

[21] Y. Hu *et al.*, "Online two-section PV array fault diagnosis with optimized voltage sensor locations," *IEEE Trans. Ind. Electron.*, 62, vol. 11, pp. 7237–7246, Nov. 2015, doi: 10.1109/TIE.2015.2448066.

[22] N. L. Georgijevic, M. V. Jankovic, S. Srdic, and Z. Radakovic, "The detection of series arc fault in photovoltaic systems based on the arc current entropy," *IEEE Trans. Power Electron.*, vol. 31, vol. 8, pp. 5917–5930, Aug. 2016, doi: 10.1109/TPEL.2015.2489759.

[23] M. K. Alam, F. H. Khan, J. Johnson, and J. Flicker, "PV arc-fault detection using spread spectrum time domain reflectometry (SSTDR)," in *Proc. 2014 IEEE Energy Convers. Congr. Expo.*, Sep. 2014, pp. 3294–3300, doi: 10.1109/ECCE.2014.6953848.

[24] K. A. Kim, G. S. Seo, B. H. Cho, and P. T. Krein, "Photovoltaic hot-spot detection for solar panel substrings using AC parameter characterization," *IEEE Trans. Power Electron.*, vol. 31, vol. 2, pp. 1121–1130, Feb. 2016, doi: 10.1109/TPEL.2015.2417548.

[25] S. V. Dhople, A. Davoudi, A. D. DomÃnguez-GarcÃa, and P. L. Chapman, "A unified approach to reliability assessment of multiphase dc-dc converters in photovoltaic energy conversion systems," *IEEE Trans. Power Electron.*, vol. 27, vol. 2, pp. 739–751, Feb. 2012, doi: 10.1109/TPEL.2010.2103329.

[26] E. Koutroulis and F. Blaabjerg, "Design optimization of transformerless grid-connected PV inverters including reliability," *IEEE Trans. Power Electron.*, vol. 28, vol. 1, pp. 325–335, Jan. 2013, doi: 10.1109/TPEL.2012.2198670.

[27] S. E. D. Leon-Aldaco, H. Calleja, F. Chan, and H. R. JimÃ©nez-Grajales, "Effect of the mission profile on the reliability of a power converter aimed at photovoltaic applications—A case study," *IEEE Trans. Power Electron.*, vol. 28, vol. 6, pp. 2998–3007, Jun. 2013, doi: 10.1109/TPEL.2012.2222673.

[28] E. Ribeiro, A. J. M. Cardoso, and C. Boccaletti, "Fault-tolerant strategy for a photovoltaic dc-dc converter," *IEEE Trans. Power Electron.*, vol. 28, vol. 6, pp. 3008–3018, Jun. 2013, doi: 10.1109/TPEL.2012.2226059.

[29] S. E. D. Leon-Aldaco, H. Calleja, and J. A. Alquicira, "Reliability and mission profiles of photovoltaic systems: A fides approach," *IEEE Trans. Power Electron.*, vol. 30, vol. 5, pp. 2578–2586, May 2015, doi: 10.1109/TPEL.2014.2356434.

[30] P. D. Reigosa, H. Wang, Y. Yang, and F. Blaabjerg, "Prediction of bond wire fatigue of IGBTs in a PV inverter under a long-term operation," *IEEE Trans. Power Electron.*, vol. 31, vol. 10, pp. 7171–7182, Oct. 2016, doi: 10.1109/TPEL.2015.2509643.

[31] G. S. Seo, K. C. Lee, and B. H. Cho, "A new DC anti-islanding technique of electrolytic capacitor-less photovoltaic interface in dc distribution systems," *IEEE Trans. Power Electron.*, vol. 28, vol. 4, pp. 1632–1641, Apr. 2013, doi: 10.1109/TPEL.2012.2208226.

[32] Y. Zhou, H. Li, and L. Liu, "Integrated autonomous voltage regulation and islanding detection for high penetration PV applications," *IEEE Trans. Power Electron.*, vol. 28, vol. 6, pp. 2826–2841, Jun. 2013, doi: 10.1109/TPEL.2012.2218288.

[33] F. A. S. Neves, M. Carrasco, F. Mancilla-David, G. M. S. Azevedo, and V. S. Santos, "Unbalanced grid fault ride-through control for single-stage photovoltaic inverters," *IEEE Trans. Power Electron.*, vol. 31, vol. 4, pp. 3338–3347, Apr. 2016, doi: 10.1109/TPEL.2015.2453275.

[34] X. Chen and Y. Li, "An islanding detection method for inverter-based distributed generators based on the reactive power disturbance," *IEEE Trans. Power Electron.*, vol. 31, vol. 5, pp. 3559–3574, May 2016, doi: 10.1109/TPEL.2015.2462333.

[35] M. Earley, C. Coache, G. Moniz, and M. Cloutier, *National Electrical Code Handbook 2014* (International Electrical Code Series), National Fire Protection Association, Quincy, MA, USA, 2013. [Online]. Available: https://books.google.com/books?id=F4BNnwEACAAJ

[36] W. Bower and J. Wiles, "Investigation of ground-fault protection devices for photovoltaic power system applications," in *Proc. IEEE 28th Photovolt. Spec. Conf.*, 2000, pp. 1378–1383.

[37] W. I. Bower and J. C. Wiles, "Analysis of grounded and ungrounded photovoltaic systems," in *Proc. IEEE 24th Photovolt. Spec. Conf.*, 1994, vol. 1, pp. 809–812.

[38] A. McEvoy, T. Markvart, L. Castaner, T. Markvart, and L. Castaner, *Practical Handbook of Photovoltaics: Fundamentals and Applications*. Elsevier, 2003. [Online]. Available: https://books.google.com/books?id=E2BAosEwDfQC

[39] J. M. Shen, H. L. Jou, and J. C. Wu, "Novel transformerless grid-connected power converter with negative grounding for photovoltaic generation system," *IEEE Trans. Power Electron.*, vol. 27, vol. 4, pp. 1818–1829, Apr. 2012, doi: 10.1109/TPEL.2011.2170435.

[40] M. G. Villalva, J. R. Gazoli, and E. R. Filho, "Comprehensive approach to modeling and simulation of photovoltaic arrays," *IEEE Trans. Power Electron.*, vol. 24, vol. 5, pp. 1198–1208, May 2009, doi: 10.1109/TPEL.2009.2013862.

[41] J. J. Soon and K. S. Low, "Photovoltaic model identification using particle swarm optimization with inverse barrier constraint," *IEEE Trans. Power Electron.*, vol. 27, vol. 9, pp. 3975–3983, Sep. 2012, doi: 10.1109/TPEL.2012.2188818.

[42] Y. Hu, J. Zhang, J. Wu, W. Cao, G. Y. Tian, and J. L. Kirtley, "Efficiency improvement of nonuniformly aged PV arrays," *IEEE Trans. Power Electron.*, vol. 32, vol. 2, pp. 1124–1137, Feb. 2017, doi: 10.1109/TPEL.2016.2544842.

[43] E. Dallago, D. G. Finarelli, U. P. Gianazza, A. L. Barnabei, and A. Liberale, "Theoretical and experimental analysis of an MPP detection algorithm employing a single-voltage sensor only and a noisy signal," *IEEE Trans. Power Electron.*, vol. 28, vol. 11, pp. 5088–5097, Nov. 2013, doi: 10.1109/TPEL.2013.2245921.

[44] S. Sajadian and R. Ahmadi, "Model predictive-based maximum power point tracking for grid-tied photovoltaic applications using a z-source inverter," *IEEE Trans. Power Electron.*, vol. 31, vol. 11, pp. 7611–7620, Nov. 2016, doi: 10.1109/TPEL.2016.2537814.
[45] S. M. R. Tousi, M. H. Moradi, N. S. Basir, and M. Nemati, "A function-based maximum power point tracking method for photovoltaic systems," *IEEE Trans. Power Electron.*, vol. 31, vol. 3, pp. 2120–2128, Mar. 2016, doi: 10.1109/TPEL.2015.2426652.
[46] C. Konstantopoulos and E. Koutroulis, "Global maximum power point tracking of flexible photovoltaic modules," *IEEE Trans. Power Electron.*, vol. 29, vol. 6, pp. 2817–2828, Jun. 2014, doi: 10.1109/TPEL.2013.2275947.
[47] M. Andresen, G. Buticchi, and M. Liserre, "Thermal stress analysis and MPPT optimization of photovoltaic systems," *IEEE Trans. Ind. Electron.*, vol. 63, vol. 8, pp. 4889–4898, Aug. 2016, doi: 10.1109/TIE.2016.2549503.
[48] S. Lyden and M. E. Haque, "A simulated annealing global maximum power point tracking approach for PV modules under partial shading conditions," *IEEE Trans. Power Electron.*, vol. 31, vol. 6, pp. 4171–4181, Jun. 2016, doi: 10.1109/TPEL.2015.2468592.
[49] C. Manickam, G. P. Raman, G. R. Raman, S. I. Ganesan, and N. Chilakapati, "Fireworks enriched p o algorithm for GMPPT and detection of partial shading in PV systems," *IEEE Trans. Power Electron.*, vol. 32, vol. 6, pp. 4432–4443, Jun. 2017, doi: 10.1109/TPEL.2016.2604279.
[50] M. A. Ghasemi, H. M. Forushani, and M. Parniani, "Partial shading detection and smooth maximum power point tracking of PV arrays under PSC," *IEEE Trans. Power Electron.*, vol. 31, vol. 9, pp. 6281–6292, Sep. 2016, doi: 10.1109/TPEL.2015.2504515.
[51] F. Rong, X. Gong, and S. Huang, "A novel grid-connected PV system based on MMC to get the maximum power under partial shading conditions," *IEEE Trans. Power Electron.*, vol. 32, vol. 6, pp. 4320–4333, Jun. 2017, doi: 10.1109/TPEL.2016.2594078.
[52] C. M. Furse, Y. Chung, C. Lo, and P. Pendayala, "A critical comparison of reflectometry methods for location of wiring faults," *Smart Structures Syst.*, vol. 2, no. 1, pp. 25–46, 2006.
[53] P. Smith, C. Furse, and J. Gunther, "Analysis of spread spectrum time domain reflectometry for wire fault location," *IEEE Sensors J.*, vol. 5, vol. 6, pp. 1469–1478, Dec. 2005, doi: 10.1109/JSEN.2005.858964.
[54] J. Reis, A. L. Castro, J. C. Costa, J. R. Riu, and K. Ericson, "Sequence and spread spectrum time domain reflectometry for transmission line analysis," in *Proc. Optics East*, 2007, pp. 67 760L–67 760L.
[55] C. Furse, P. Smith, C. Lo, Y. C. Chung, P. Pendayala, and K. Nagoti, "Spread spectrum sensors for critical fault location on live wire networks," *Structural Control Health Monitoring*, vol. 12, no. 3-4, pp. 257–267, 2005.
[56] C. Furse, P. Smith, M. Safavi, and C. Lo, "Feasibility of spread spectrum sensors for location of arcs on live wires," *IEEE Sensors J.*, vol. 5, vol. 6, pp. 1445–1450, Dec. 2005, doi: 10.1109/JSEN.2005.858900.
[57] T. Takashima, J. Yamaguchi, K. Otani, T. Oozeki, K. Kato, and M. Ishida, "Experimental studies of fault location in PV module strings," *Sol. Energy Mater. Sol. Cells*, vol. 93, no. 6, pp. 1079–1082, 2009.
[58] T. Takashima, J. Yamaguchi, and M. Ishida, "Fault detection by signal response in PV module strings," in *Proc. IEEE 33rd Photovolt. Spec. Conf.*, May 2008, pp. 1–5, doi: 10.1109/PVSC.2008.4922843.
[59] T. Takashima, J. Yamaguchi, K. Otani, K. Kato, and M. Ishida, "Experimental studies of failure detection methods in PV module strings," in *Proc. 2006 IEEE 4th World Conf. Photovolt. Energy Conf.*, May 2006, vol. 2, pp. 2227–2230, doi: 10.1109/WCPEC.2006.279952.
[60] L. Schirone, F. P. Califano, U. Moschella, and U. Rocca, "Fault finding in a 1 mW photovoltaic plant by reflectometry," in *Proc. Photovolt. Spec. Conf.*, Dec. 1994, vol. 1, pp. 846–849, doi: 10.1109/WCPEC.1994.520093.
[61] C. Miquel, "Frequencies studies applied to photovoltaic modules," M.S. thesis, KTH Royal Institute of Technology, Stockholm, Sweden, 2011.
[62] F. T. Ulaby, E. Michielssen, and U. Ravaioli, *Fundamentals of Applied Electromagnetics*, 6th ed. Upper Saddle River, NJ, USA: Prentice-Hall, Apr. 2010.
[63] P. D. Dresselhaus, E. J. Dean, A. H. Worsham, J. X. Przybysz, and S. V. Polonsky, "Modulation and demodulation of 2 GHz pseudo random binary sequence using SFQ digital circuits," *IEEE Trans. Appl. Supercond.*, vol. 9, vol. 2, pp. 3585–3589, Jun. 1999, doi: 10.1109/77.783805.
[64] J. Gunther, D. Dosibhatla, and C. Furse, "Digital spread spectrum methods and apparatus for testing aircraft wiring," US Patent 7 069 163, Jun. 27, 2006.
[65] C. Furse and P. Smith, "Method and apparatus for characterizing a signal path carrying an operational signal," US Patent 7 250 772, Jul. 31 2007.
[66] R. Harrison, C. Furse, and C. Sharma, "Reflectometry test system using a sliding pseudo-noise reference," US Patent 7 548 071, Jun. 16, 2009.

Sourov Roy (S'17) received the B.Sc. degree in electrical and electronic engineering from the Bangladesh University of Engineering and Technology, Dhaka, Bangladesh, in 2012. He is currently working toward the Ph.D. degree with the Department of Computer Science and Electrical Engineering, University of Missouri–Kansas City, Kansas City, MO, USA.

He was a Lecturer with the Daffodil International University, Bangladesh, from 2012 to 2013. From 2013 to 2014, he was with Civil Aviation Authority, Bangladesh, as an Assistant Engineer. He also served Bangladesh Power development Board and Dhaka Power Distribution Company Limited, Bangladesh, as Assistant Engineer from 2014 to 2015. His current research interests include power converter reliability estimation using spread spectrum time-domain reflectometry, and energy harvesting and power conditioning circuits for biomedical applications.

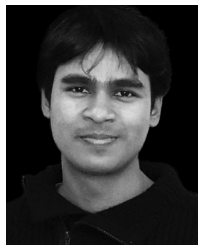

Mohammed Khorshed Alam (M'16) received the B.Sc. degree from the Bangladesh University of Engineering and Technology, Dhaka, Bangladesh and the Ph.D. degree from the University of Utah, Salt Lake City, UT, USA, in 2009 and 2014, respectively, all in electrical engineering.

Since 2015, he has been working as a Power Electronics Engineer at Ford Motor Company, Dearborn, MI, USA. He has authored more than 20 technical publications and more than 15 pending US patents. His research interests include dc–dc converters, traction inverter, photovoltaics, and reliability.

Faisal Khan (SM'13) received the B.Sc. degree in electrical engineering from the Bangladesh University of Engineering and Technology, Dhaka, Bangladesh, in 1999, the M.S. degree in electrical engineering from Arizona State University, Tempe, AZ, USA, in 2003, and the Ph.D. degree in electrical engineering from the University of Tennessee, Knoxville, TN, USA, in 2007.

From 2007 to 2009, he was with Electric Power Research Institute, as a Senior Power Electronics Engineer. From 2009 to 2014, he was with the Electrical and Computer Engineering Department, University of Utah, as an Assistant Professor. Since 2015, he has been with the Department of Computer Science and Electrical Engineering, University of Missouri–Kansas City, Kansas City, MO, USA, as an Associate Professor. His major research interest include characterizing degradation/aging in power converters using spread spectrum time domain reflectometry. He also works with micropower converters for biomedical applications.

Prof. Khan is an Associate Editor of the IEEE TRANSACTIONS ON POWER ELECTRONICS.

Jay Johnson (M'12) received the B.S. degree from the University of Missouri-Rolla, Rolla, MO, USA, and the M.S. degree from the Georgia Institute of Technology, Atlanta, GA, USA, in 2009, both in mechanical engineering.

He is a Principal Member of the Technical Staff, Sandia National Laboratories, Albuquerque, NM, USA. He has been researching renewable energy and energy efficiency systems for more than a decade- in which time he led the Sandia Arc-Fault and Ground Fault Detection and Mitigation Program for five years. He now heads several multidisciplinary, renewable energy, and grid integration research projects in the areas of distributed energy resource control, optimization, interoperability, and cybersecurity.

Jack Flicker (M'13) is a Senior Member of the Technical Staff, Sandia National Laboratories, Albuquerque, NM, USA. He has been carrying out research on power electronics and photovoltaics safety and reliability for six years. He has authored more than 15 publications on system reliability and fault detection/mitigation in photovoltaic arrays and more than 50 total publications on photovoltaic systems and power electronics.